Title: The correlation between bubble-enhanced HIFU heating and cavitation power

Authors: Caleb H. Farny, R. Glynn Holt, Ronald A. Roy

Affiliation: Department of Mechanical Engineering, Boston University, Boston MA

Correspondence: Department of Radiology, Harvard Medical School, Brigham and Women's Hospital, 221 Longwood Ave, Boston MA 02115

Email: cfarny@bwh.harvard.edu

Abstract: It has been established that while the inherent presence of bubbles increases heat generation due to scattering and absorption, inertial cavitation is responsible for significantly-higher heating rates during high-intensity focused ultrasound (HIFU) application. The contribution of bubble-induced heating can be an important factor to consider, as it can be several times greater than the expected heat deposition from absorption of energy from the primary ultrasound field. The temperature and cavitation signal near the focus were measured for 5.5-s continuous wave 1.1-MHz HIFU sonications in tissue mimicking phantoms. The measured temperature was corrected for heating predicted from the primary ultrasound absorption to isolate the temperature rise from the bubble activity. The temperature rise induced from cavitation correlates well with a measurement of the instantaneous "cavitation power" as indicated by the mean square voltage output of a 15-MHz passive cavitation detector. The results suggest that careful processing of the cavitation signals can serve as a proxy for measuring the heating contribution from inertial cavitation.

INTRODUCTION

High-intensity focused ultrasound (HIFU) shows great promise as a noninvasive thermal therapy for tumor ablation. Ablation relies on generation of heat from the absorption of spatially-localized acoustic energy from the focused sound source, and may be achieved by heating tissue to a sufficient temperature for a sufficiently-long time duration. The temperature history during sonication, often referred to as a thermal dose [1], [2], has been used to indicate when tissue ablation has likely occurred [3], [4]. A significant barrier to successful HIFU application is the difficulty in noninvasively measuring the temperature in the treatment region and thus, it is difficult to assess dose

and determine when to end treatment. This is further complicated by the possible nucleation and subsequent interaction of bubbles within the sound field, which can lead to a variety of physical effects. One such effect is supplemental heat generation from inertial cavitation [5]-[9], which is characterized by unstable growth followed by inertially-driven collapse and concomitant broad-band acoustic emissions. The ability to account for heating from cavitation would greatly improve HIFU treatment monitoring.

Acoustic cavitation, broadly defined as the nucleation and/or driven pulsations of a bubble in the presence of a sound field, was first associated with enhanced heating by Lele [5], and is reviewed by Leighton [6]. Here 'enhanced heating' refers to heat generation over and above that expected from classical thermo-viscous absorption of the ultrasound energy. Lele used a 2.7 MHz HIFU source to sonicate fresh calf liver over a range of intensities and measured temperature and acoustic emissions associated with cavitation. Temperature rise at intensities too low to induce cavitation was modest and predictable. So-called stable cavitation was detected at slightly higher intensities via the presence of sub-harmonic emissions and the temperature rise was slightly higher than expected. At yet higher intensities, both stable and inertial cavitation was detected and the temperature rose dramatically. Lele theorized that the high heating rates were due to inertial cavitation effects.

Hynynen [7] measured temperature rise and broadband noise generation during *in vivo* dog thigh sonication as a function of HIFU frequency (0.246 – 1.68 MHz), and intensity. Measured temperature rise had a linear dependence on intensity at low intensities, as expected, but increased substantially at higher intensities when a threshold-type increase in broadband emissions was concurrently detected, an indication of inertial

cavitation. Razansky *et al.* [10] measured temperature rise in a viscous liquid layer containing Optison™ during 1 or 3.2 MHz sonication, at pressures lower than the reported inertial cavitation threshold [11]. They found that heating from stable cavitation was more efficient for bubble populations that were not destroyed during sonication, although heating at clinical Optison™ dosages for the same sonication parameters was minimal.

Holt and Roy [8] used a 1 MHz HIFU source for 0.5 – 10 s continuous wave (CW) exposures in agar tissue-mimicking phantoms at multiple pressures. Temperature was measured with thermocouples embedded at multiple positions adjacent to the HIFU focus. The temperature rise at low pressures corresponded to heating from classical thermo-viscous absorption from the 1 MHz energy, but above 1.4 MPa the heating was significantly greater than that predicted by the classical model, which does not account for bubble-related phenomena. The elevated heating was attributed to cavitation, as the onset of the elevated temperature rise coincided closely with the onset of elevated sub-harmonic and broadband signals at a "cavitation nucleation threshold pressure" of 1.4 MPa. The authors recognized that cavitation plays a role in lesion distortion but also argued that if controlled properly, enhanced heating caused by cavitation could enhance the speed and efficacy of HIFU treatment.

In Hilgenfeldt *et al.* [9], Holt and Roy [8], and ensuing investigations by Edson [12], [13], and Yang *et al.* [14], modeling of the bubble dynamics revealed that two mechanisms can explain the additional heat generation: viscous damping from radial motion of stable cavities, and local absorption of the acoustic emissions from inertial bubble collapses. Hilgenfeldt *et al.* showed that for short-pulse insonation (similar to that

employed in diagnostic ultrasound) in a blood-like medium, viscous damping had little effect on temperature rise near the bubble, while heat dissipation from absorption of radiated emissions could result in temperature rises of up to 100 K near the bubble wall. Edson and Yang *et al.* determined numerically that both mechanisms were capable of producing similar levels of heating, but for different ranges of viscosity and equilibrium bubble radius: inertial cavitation is dominant for lower viscosities and sub-resonant-size bubbles whereas heating from stable cavitation occurs for larger bubbles and high viscosities. Employing a 15-MHz center frequency passive cavitation detector (PCD) configured to selectively detect broadband emissions from inertial cavitation, Edson also showed that the occurrence of enhanced heating corresponded with the onset of broadband noise and concluded that local absorption of inertial cavitation noise was most likely the dominant mechanism in bubble-enhanced heating in his experiments. This conclusion was reinforced by Yang *et al.*, whose simulations included the effects of shape mode instabilities and showed that the maximum equilibrium size a bubble can attain without breaking up is dependent on the driving pressure amplitude, acoustic frequency, medium viscosity and dissolved gas saturation level. For the experimental conditions employed by Edson, only sub-resonant bubbles are "permitted" and thus the only avenue available for significant enhanced heating is inertial cavitation.

Results from these investigations suggest strongly that heating from cavitation encountered in HIFU, when present, is most likely due to the absorption of broadband "secondary acoustic emissions" from inertial cavitation. We hypothesize that "emission diagnostics" - the passive detection and interpretation of acoustic emissions from inertial cavitation - can serve as a non-invasive, real time indicator of excess heat generation

from inertial cavitation effects. The main goal of this study was to evaluate, in a controlled setting, the relationship between inertial cavitation emissions and heat generation from inertial cavitation. Active and passive cavitation detection methods have been used previously to correlate cavitation with associated mechanical effects, such as hemolysis [15]-[17] and tissue destruction [18], but not directly with heating rates. Herein we report results from tissue mimicking phantom experiments that employ known propagation conditions and a well-characterized medium to isolate bubble heating from that due to thermo-viscous absorption of the incident 1.1-MHz HIFU field. The study found that cavitation power correlates well with the rate of temperature rise associated with energy deposition from inertial cavitation.

THEORY

We employed a combination of experiments and modeling to assess the relationship between bubble heating and cavitation noise. Starting with a calibrated 1.1-MHz sound source and a well-characterized tissue phantom, we computed the pressure and temperature fields expected from thermo-viscous heating alone, taking care to verify that the model and experimental results are in agreement for pressure amplitudes low enough to preclude cavitation activity. At higher pressures, the difference between the measured and computed temperature rise (the former is always greater) can then be ascribed to bubbles and compared with cavitation diagnostics. Here we were careful to consider that an additional source of accelerated heating – that due to the enhanced absorption of shocked wavefronts [19] – is not a factor given the relatively low pressures employed in this study.

The Pressure Field

The pressure output from the sound source was modeled to determine time-averaged, spatially-dependent ultrasound power deposition from which conventional thermo-viscous heating rates could be calculated. Following Hallaj [20] and Edson [12], we employed a FDTD solution (described below) of the classical Westervelt equation [21], [22],

$$\nabla^2 p - \frac{1}{c^2}\frac{\partial^2 p}{\partial t^2} + \frac{\delta}{c^4}\frac{\partial^3 p}{\partial t^3} + \frac{\beta}{\rho c^4}\frac{\partial^2 p^2}{\partial t^2} = 0 \ . \qquad (1)$$

Here, p is the acoustic pressure, c is the sound speed, t is the time, δ is the local acoustic diffusivity, β is the nonlinearity coefficient and ρ is the density. The acoustic absorption α, is related to the acoustic diffusivity by $\alpha = \frac{\delta \omega^2}{2c^3}$, where ω is the angular frequency. Equation (1) describes wave propagation through a weakly nonlinear thermo-viscous fluid and accounts for losses from thermal conduction and viscosity in the third term and nonlinear distortion in the fourth term. The formula approximates the nonlinearity by taking into account the effects that accumulate with distance but not the smaller local effects, which can be neglected for focused sound sources [22]. The material-dependent parameters required by the model, such as the absorption, sound speed, nonlinearity coefficient, and density, were determined from an independent characterization of the medium.

The Temperature Field

HIFU-induced heat generation was modeled using a modified Pennes heat transfer equation [23]. Two heat sources (described below) are present in our system: (1) deposited energy due to absorption of the primary HIFU field q_{HIFU} and (2) energy from

cavitation enhanced heating q_c. Both are cast as power density terms in the standard transport equation,

$$\rho C \frac{\partial T(r,t)}{\partial t} = K\nabla^2 T(r,t) + q_{HIFU}(r) + q_c(r,t), \tag{2}$$

where C is the heat capacity and K is the thermal conductivity of the medium.

Heating From HIFU in the Absence of Cavitation

Upon computing the HIFU pressure field using Eq. (1), the determination of q_{HIFU} followed using the standard expression for the acoustic power dissipated per unit volume due to plane wave propagation in a thermo-viscous fluid [24],

$$q_{HIFU} \approx \frac{2\alpha}{\rho c \omega^2}\left(\frac{\partial p}{\partial t}\right)^2. \tag{3}$$

The plane wave approximation holds in the HIFU focus, which is where most of the heating occurs. In the event where cavitation does not occur or its effects have been isolated, q_{HIFU} is the only relevant source term and the heat transport equation takes the form

$$\rho C \frac{\partial T_{HIFU}(r,t)}{\partial t} = K\nabla^2 T_{HIFU}(r,t) + \frac{2\alpha}{\rho c \omega^2}\left(\frac{\partial p}{\partial t}\right)^2. \tag{4}$$

From this relationship, the resulting temperature field was determined via FDTD simulation.

Heating from Cavitation Alone

Strictly speaking, three mechanisms exist by which an acoustically-driven bubble can convert acoustical energy into thermal energy [25], [26]: thermal damping, viscous damping, and absorption of the radiated pressure wave induced by inertial cavity collapse, which we refer to as a "secondary acoustic emission." It is assumed that the

bubble radius is on the order of a micron or smaller, which at the fundamental sonication frequency of 1.1 MHz leads to isothermal oscillations and minimal heating from thermal damping. A comparison of the damping mechanisms for low-amplitude forcing described by Prosperetti [26] shows that heating from thermal damping at 1.1 MHz and radii ranging from 0.01 – 1 μm is approximately 100x lower than the contribution from viscous damping. This effect has been demonstrated to be minimal for high-amplitude forcing as well [27], [28]. Edson [12], [13] and Yang *et al.* [14] showed that absorption of the broadband secondary acoustic emission was the dominant bubble-related heating mechanism for the acoustic parameters used in this study. It follows that the cavitation heating source term given in Eq. (2), q_c, is due to absorbed inertial cavitation energy and we anticipate some correlation between bubble-related heating rates and measured cavitation emissions.

To determine the radiated pressure field, we assume that a bubble located at r undergoes a perfectly spherical collapse, such that the radiated pressure is

$$p_{rad}(r, r_b, t) = \frac{\rho R}{r_b}\left(2\dot{R}^2 + R\ddot{R}\right), \tag{5}$$

where r_b is the distance from the bubble, and $R, \dot{R}, \ddot{R}$ are the bubble radius, velocity and acceleration, respectively. The radiated energy is obtained by first determining the time-averaged radiated intensity I_{rad},

$$I_{rad}(r, r_b) = \frac{\left\langle {p_{rad}}^2(r, r_b, t)\right\rangle_\tau}{\rho c} = \frac{p_{rms}^2(r, r_b)}{\rho c}. \tag{6}$$

where τ is the time interval over which the rms pressure is evaluated. The maximum radiated power $D_{rad}^{\max}$ available for absorption is [9]

$$D_{rad}^{\max}(r) = 4\pi r_b^2 \times I_{rad}(r, r_b). \tag{7}$$

The *actual* power deposited will depend on the path length over which the acoustic emission is absorbed, so the final expression for power deposited by the bubble within a volume subtended by a sphere of radius *r'* is

$$D_{rad}^{abs}(r, r') = D_{rad}^{\max}(r)\left(1 - e^{-2\alpha(f)r'}\right), \tag{8}$$

where loss due to attenuation has been included. The spatial average power density over this volume corresponds directly to q_b and is approximated by

$$q_{bubbles} = q_{rad}^{abs}(r) = \frac{4}{3\pi r'^3} D_{rad}^{abs}(r, r') \ , \tag{9}$$

yielding the following equation describing heat transport from cavitation alone,

$$\rho C \frac{\partial T_c(r,t)}{\partial t} = K\nabla^2 T_c(r,t) + \frac{4}{3\pi r'^3} D_{rad}^{abs}(r, r') \ . \tag{10}$$

Finite-Difference Time Domain Solution

The FDTD model and codes employed were adapted from previous work by Hallaj [20] and Edson [12], to which the reader is referred for the complete details. The pressure solution was solved on a 5 x 10 cm grid with a 100 μm spatial step size (~13 steps per wavelength) and the spherical source geometry allowed us to use an axi-symmetric approximation to halve the grid size to reduce computation time. The pressure was solved using a 10 ns time step over 100 cycles, the time required for the wavefront to propagate throughout the grid, at which point the pressure was deemed to be steady state.

The steady state pressure was used to determine the time-averaged power density, which was used as the heat source in the temperature solution, Eq. 2. The temperature field was computed over the exposure duration employed in the experiment (5.5 s), plus three seconds to monitor cooling. A 1 ms time step was used to reduce computation time,

due to the slower time scale associated with thermal diffusion. The temperature field was solved over a 1.5 x 5 cm grid, corresponding to the size of the phantom, with a 100-μm step size. This method for temperature simulation was compared against experimental measurements at pressures below the cavitaiton threshold using a similar phantom, sound source, and temperature acquisition by Huang [29]. The model results demonstrated excellent agreement with the experimental measurements.

Relationship Between Bubble Heating and Bubble Noise

The cavitation noise sensor described below, often referred to as a "passive cavitation detector" or PCD, possesses limited bandwidth and a sensing volume that is smaller than the volume of the HIFU transducer focus. Moreover, the bubble heating source term is highly localized and the associated temperature field will depend on conduction as well as the spatial distribution of cavitation activity. If q_{rad}^{abs} is evaluated over short durations where conduction effects are small, the broadband cavitation signal may still describe the spatially-averaged heating rate associated with cavitation within the sensing volume. Ignoring heat conduction and assuming that the power density associated with cavitation is uniform over the sensing volume, Eqs. (6 - 10) yield the following approximate expression for bubble-induced heating in this volume:

$$\rho C \frac{\partial T_b(r_{sv},t)}{\partial t} = \frac{4}{3\pi r_{pcd}^{\ 3}} D_{rad}^{abs}(r_{sv},r_{pcd}), \tag{11}$$

where r_{sv} is the location of the sensing volume and r_{pcd} is the equivalent spherical radius of the sensing volume. Solving for the heating rate and assuming that the geometry of the detection region as well as the acoustical and thermodynamic properties of the medium do not change in the time frame of the measurement yields:

$$\left.\frac{\partial T_b(r_{sv},t)}{\partial t}\right|_{\tau} = A\left\langle {p_{rad}}^2(r_{sv},t)\right\rangle_{\tau} = A\cdot p_{rms}^2(r_{sv})\Big|_{\tau}, \qquad (12)$$

where A is a proportionality constant, and τ is assumed to be small compared to the relevant diffusion time scale. Heating rates from inertial cavitation activity can therefore be estimated by measuring the mean square noise pressure generated within the sensing volume of the PCD, which in turn is linearly related to the mean square voltage signal from the PCD transducer, V_{rms}^2.

An ideal scenario would be to measure the temperature rise produced by inertial cavitation directly, rather than the heating rate. However, such an approach would be impractical for it would require knowledge of the spatial distribution of the cavitation signal throughout the heated region and over the entire bandwidth of the radiated emissions. In addition it would be necessary to account for changes in acoustical and thermal properties in the medium due to the presence of bubbles, and calibrate the PCD to yield absolute pressure measurements for a given detection geometry. While the proportionality constant A will be specific to the tissue type and PCD system, establishment of the validity this approach will show that *changes* and *trends* in bubble-assisted heating rates may still be assessed by monitoring the changing amplitude of the cavitation emissions. This relatively simple measurement could then be used to non-invasively guide HIFU treatment in real time and provide feedback regarding when and where bubble-enhanced heating could be playing a role in lesion formation.

MATERIALS AND METHODS

Rationale

The experiment consisted of comparing temperature measurements, adjusted for simulated thermoviscous heating, with broadband emissions measured from a PCD. The temperature was measured with a thermocouple embedded in a gel phantom exposed to HIFU radiation at a position r_{TC}, which lay 0.5 mm from the beam axis in the HIFU focal plane. We assumed that heat deposition in the sensing region was generated by both direct HIFU heating and cavitation-enhanced heating, yielding the following estimate of the temperature rise induced by cavitation:

$$\frac{\Delta T_b(t)}{\Delta t} = \frac{T_{TC}(t)}{\Delta t} - \frac{\Delta T_{HIFU}(t, r_{TC})}{\Delta t}. \tag{13}$$

Here, T_{TC} is the measured thermocouple temperature and T_{HIFU} is the temperature obtained from the FDTD solution to the bubble-free heat transfer equation at the position of the thermocouple. The timescale Δt for the analysis was 20 ms and is discussed below.

A focused PCD was positioned confocal to the HIFU transducer so as to monitor the cavitation noise field. The square of the rms voltage from the PCD is proportional to the radiated power incident on the receiver, which is proportional to the radiated power emanating from the PCD sensing volume. Equation 12 becomes

$$\left.\frac{\partial T_b}{\partial t}\right|_{\tau} = B \cdot \left. V_{rms}^2 \right|_{\tau}, \tag{14}$$

where B is an experimentally-determined proportionality constant that includes the physical properties of the medium, the sensitivity of the PCD, and the dimensions of the sensing volume. The model assumption is simple: the thermal power deposited in the sensing volume of the detector should be proportional to the mean square voltage measured by the PCD. While it does not have the proper dimensions to be termed a

power, the right side of Eq. 14 will be referred to as the *cavitation power* for the sake of notational convenience.

HIFU Transducer

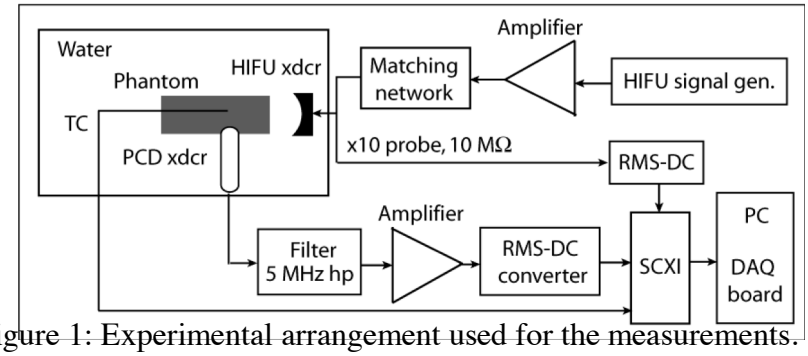

Figure 1: Experimental arrangement used for the measurements.

The experimental arrangement employed in these measurements is shown in Fig. 1. A single-element spherically-focused piezoceramic transducer (focal length = 62 mm; aperture = 70 mm; –6-dB beamwidth = 1.8 mm; H-102, Sonic Concepts, Seattle, WA) with a 20-mm hole and nominal center frequency of 1.1 MHz was employed as the HIFU source. A function generator (33120A, Agilent Technologies, Palo Alto, CA) supplied the 1.1 MHz signal which was first attenuated (-25 dB, JFW Industries, Indianapolis, IN) and amplified (60 dB, A-500, ENI, Rochester, NY) before passing through a custom matching network (Sonic Concepts). All measurements were performed in a Lucite tank (45 x 45 x 58 cm) filled with water which had been degassed, deionized and filtered (0.2-μm particulate filter, Fin-L-Filter). The temperature of the water (22 ± 2°C) was monitored with an alcohol thermometer daily.

The free field HIFU pressure was determined using a pressure calibration performed in water using a calibrated membrane hydrophone (0.2 mm diameter, model #0200, Precision Acoustics, Dorchester, UK). A comparison between the measured and

simulated pressure is shown in Ref [29]. The focal pressure in the phantom was determined by modeling the pressure field with the FDTD model using the measured phantom properties. The input voltage to the transducer was monitored by a high-impedance attenuating voltage probe. The probe signal was conditioned with a RMS-DC converter circuit (AD637, Analog Devices, Norwood, MA) and digitized at 2 kSamples/s by an 8-channel signal conditioning unit (SCXI-1120, National Instruments, Austin, TX) and 12-bit data acquisition board (AT-MIO-16E-1, National Instruments).

Passive Cavitation Detection

Inertial cavitation detection was performed with a 15-MHz focused transducer (focal length = 19 mm; aperture = 6.4 mm; -6 dB focal width = 0.29 mm; -6 dB bandwidth = 12 – 19 MHz, V313, Panametrics-NDT Corp., Waltham, MA) that was aligned perpendicular and confocal to the HIFU focus. Alignment was achieved by maximizing the echo signal from a 3.18-mm diameter brass sphere and correcting the alignment for the sphere radius. The transducer was operated in receive mode and the signal was attenuated by a variable-step attenuator (JFW Industries, Indianapolis, IN), amplified (W40D, TronTech) and filtered by a passive 5 MHz high-pass filter (F5081-FP0-B, Allen Avionics, Mineola, NY) in order to remove the incident HIFU energy scattered into the aperture of the PCD. A 5 MHz cutoff frequency eliminates the fundamental, second, third and fourth harmonic components of the HIFU signal, but higher harmonics, if present, will be detected. The signal was conditioned by a broadband RMS-DC converter (AD8361, Analog Devices, Norwood, MA) and acquired with the signal conditioning unit and data acquisition board described above. All data acquisition and analysis was performed using MATLAB (R14, The MathWorks, Natick, MA).

Temperature Sensing

The temperature was measured using a bare-wire thermocouple (Type E, 125 μm diameter, Omega, Stamford, CT). The thermocouple was aligned parallel to the HIFU transducer axis and the tip was positioned 0.5 mm lateral to the HIFU focus to reduce the possibility of bubble nucleation on the thermocouple tip. The signal was conditioned with a 4 Hz low-pass filter and 60 dB amplifier onboard the signal conditioning unit and digitized with the data acquisition board used for the HIFU driving voltage acquisition.

Tissue Mimicking Phantom

Agar-based tissue-mimicking phantoms [8] were used to simulate tissue in this study and provided a material in which cavitation and clinically-relevant temperature elevations could be produced at modest clinical HIFU pressures for short-duration sonications. 600 mL of deionized, filtered water was degassed and heated to 80°C. Once heated, 18 g of agar (Sigma-Aldrich Corp., St. Louis, MO), 0.75 g of methyl paraben (Sigma-Aldrich), 24 g of graphite (325 mesh, Mallinkdrodt, Phillipsburg, NJ) and 16 mL of n-propanol (Fisher Scientific, Hampton, NH) were added and dissolved into solution. The mixture was degassed on a hot plate with a magnetic stir bar to prevent settling and poured into a mold to cool until set. Cylindrical film canisters (31 x 47 mm) were used as molds to cast the phantom, and the phantom was positioned lengthwise along the HIFU axis during measurements. For experiments where temperature monitoring was desired, a thermocouple was directly cast into the phantom, with the thermocouple tip positioned ~15 mm from the edge of the phantom distal to the HIFU transducer.

The recipe was adjusted to match the acoustic and thermal properties of tissue, as shown in Table I, and these properties were characterized as described in Ref. [30]. The

nonlinearity coefficient β was characterized using a finite amplitude insert-substitution method [31]. The attenuation power law measured from 1 – 3.5 MHz was found to correspond to 1.6 [32].

Density (kg/m^3)	Sound Speed (m/s)	Attenuation (Np/m/MHz)	Nonlinearity coefficient β	Thermal diffusivity (mm^2/s)	Specific heat (J/kg.°C)
1003	1520	5.1	4.5	0.158	3710

Table I: Acoustic and thermal properties of the tissue phantom at room temperature.

The inertial cavitation threshold was determined through a series of measurements where the phantom was sonicated continuously from the HIFU source for 0.9 s, followed by no sonication for 120 s for cooling. The pressure was increased after each burst, ultimately covering a range of 0.8 – 2 MPa in 0.07 MPa steps. The inertial cavitation threshold was defined as the lowest pressure at which the mean amplitude of the broadband noise between 6 – 6.5 MHz (sufficiently above the filter cutoff frequency and below the sixth harmonic) was greater than three standard deviations above the mean broadband noise measured between 6 – 6.5 MHz when the sound field was turned off [33]. The threshold was determined to be about 1.4 MPa, similar to the threshold measured by Holt and Roy [8] and slightly lower than the 1.7-MPa threshold measured by Edson [12].

Exposure Protocol

Each measurement consisted of a 5.5-s, 1.1 MHz CW exposure in a phantom during which the PCD V_{rms}, thermocouple voltage and HIFU transducer excitation V_{rms} were simultaneously sampled at 2 kSamples/s. The experiment consisted of 41 measurements encompassing six focal pressure amplitudes (2.0, 2.5, 2.8, 3.3, 3.5, 4.2

MPa) in order to evaluate whether the cavitation heating efficacy changed with pressure and how this change scaled with the PCD-detected emissions. A fresh, unexposed phantom was used for each measurement.

Data Analysis

The cavitation power (RHS of Eq. 14) was compared to the rate of temperature rise (LHS of Eq. 14) by first subtracting the simulated temperature from the primary field absorption T_{HIFU} from the measured temperature T_{TC}. The rate of temperature rise due to cavitation was then calculated over time steps of $\tau = 20$ ms. The cavitation power was determined by squaring the PCD V_{rms} and computing the average of the mean square voltage over each 20 ms step. The proportionality constant B was obtained from a least-squares error fit to the entire data stream. By choosing to employ a 5 MHz high-pass filter to remove the scattered HIFU energy from the PCD signal we assumed that the unfiltered signal consisted solely of broadband energy from inertial cavitation and was not significantly impacted by any higher harmonics of the HIFU beam that may have been present. The validity of this assumption is discussed in Appendix A.

The analysis assumes negligible heat loss in the sensing region from conduction. This assumption sets the maximum time interval for evaluating V_{rms}^2. This limit is the thermal diffusion time, given by $t_\alpha = L_\alpha^2/\alpha$, where L_α is the relevant length over which the temperature gradient will cause significant heat loss and α is the thermal diffusivity in the phantom. We take L_α as the pressure-dependent radius of the "cavitation-zone", which is the region for which the HIFU pressure amplitude exceeds 1.4 MPa, the measured inertial cavitation threshold pressure for the phantom. Table II lists these length scales, as determined from the pressure simulation, and the corresponding diffusion times

for the sonication pressures employed. Our processing time step of $\Delta t = 20$ ms is indeed much smaller than any of the diffusion times listed. In addition we have assumed the sensing volume is sufficiently small so that the bubble-enhanced absorbed power density can be considered uniform.

P_{foc} (MPa)	2	2.5	2.8	3.3	3.5	4.2
L_α (mm)	0.52	0.75	0.84	0.93	0.97	1.04
t_α (s)	1.71	3.56	4.47	5.47	5.89	6.87

Table II: Bubble heating thermal diffusion times in the phantom for the HIFU pressure amplitudes employed in the measurements.

RESULTS

Two examples of the cavitation power and temperature rise are shown in Figs. 2 and 3 for $P_{foc} = 2.6$ and 2.8 MPa, respectively. The signal in panel (a) of both figures

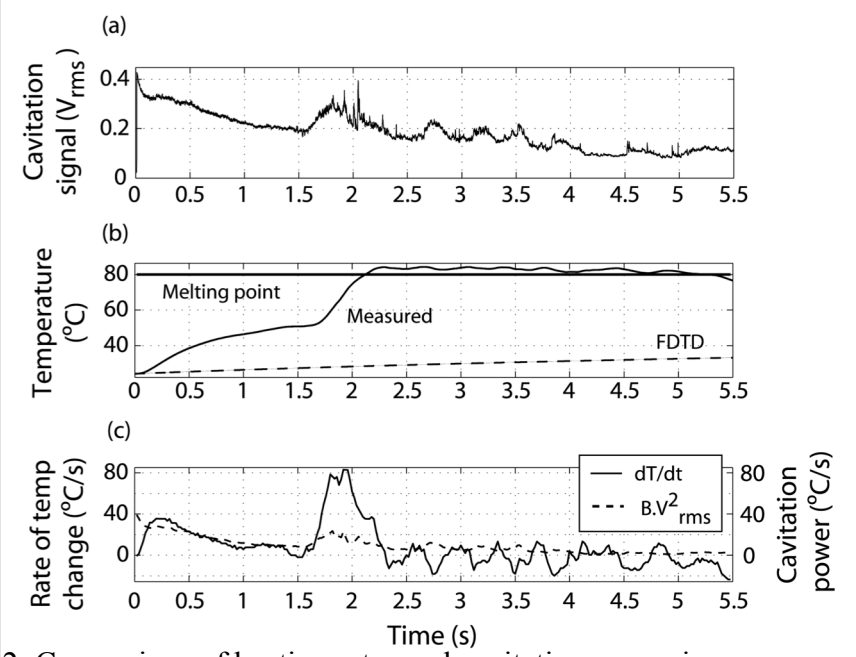

Figure 2: Comparison of heating rates and cavitation power in an agar-graphite phantom for 5.5 s CW exposures at 1.1 MHz and P_{foc}=2.6 MPa. (a) Inertial cavitation emissions measured by the PCD. (b) Measured and predicted (no bubbles) temperature rise 0.5 mm lateral to the focus. The melting point of the phantom was 80°C. (c) Bubble-generated heating rate and cavitation power.

shows a characteristic trend of decreasing cavitation over the course of sonication, while the temperature increases rapidly. Note that the measured temperature in panel (b) is several times greater than the temperature predicted from thermoviscous absorption of the HIFU energy. Also shown is the melting point of the phantom, at which point the bulk properties of the phantom may change and new phenomena such as boiling and acoustic streaming may commence.

A second feature manifested in the majority of the measurements was a dramatic increase in both the cavitation signal and temperature rise part way into sonication, seen at $t \sim 1.7$ s in Fig. 2 and to a lesser degree at 4.3 s in Fig. 3. There was no such increase in cavitation noise in measurement performed without a thermocouple imbedded in the phantom. We conclude that these sudden "bursts" of cavitation noise and concomitant

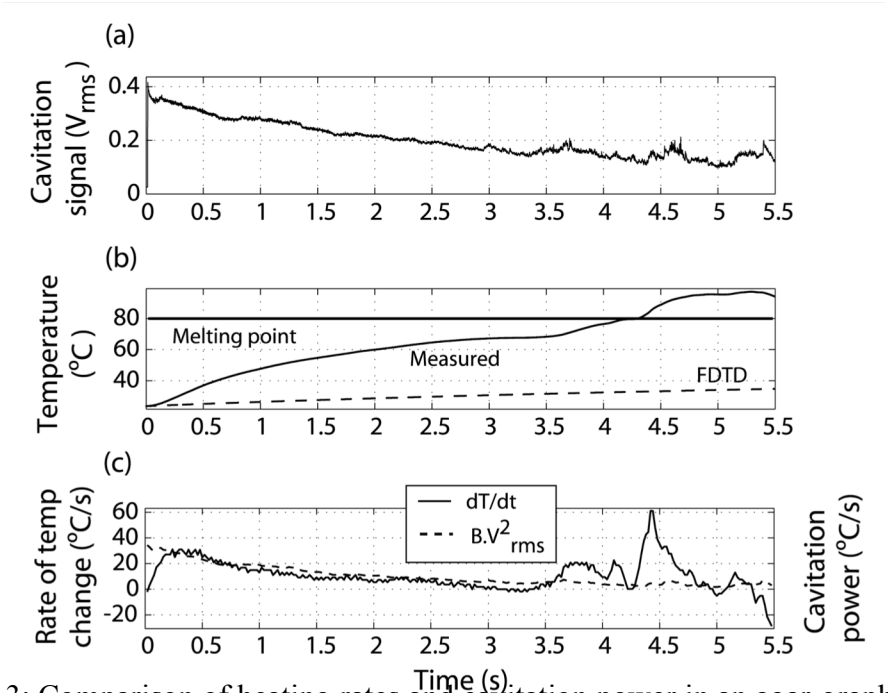

Figure 3: Comparison of heating rates and cavitation power in an agar-graphite phantom for 5.5 s CW exposures at 1.1 MHz and P_{foc}=2.8 MPa. (a) Inertial cavitation emissions measured by the PCD. (b) Measured and predicted (no bubbles) temperature rise 0.5 mm lateral to the focus. The melting point of the phantom was 80°C. (c) Bubble-generated heating rate and cavitation power.

increases in heating rates are likely due to cavitation on the thermocouple tip (or thermocouple sheath), resulting in elevated temperatures and cavitation emissions, as the spherical thermocouple tip may have acted as a preferential site for cavitation nucleation. This unfortunate artifact is due to the invasive nature of the temperature measurement scheme.

The cavitation power and rate of temperature change are compared in panel (c) for Figs. 2 and 3. The fit used in each figure corresponds to $B = 299$, the average proportionality constant for all 41 measurements. The fitted cavitation power curve shows general agreement with the temperature rise for the portion that lies between $T_{TC} \sim$ 30°C and the onset of a 'thermocouple cavitation nucleation event'. As the cavitation signal decreases over time, the rate of temperature rise from secondary acoustic heating decreases as well.

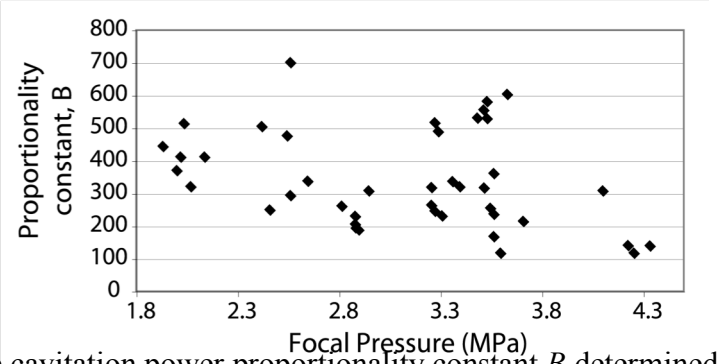

Figure 4: The cavitation power proportionality constant B determined from the least-squared error fit for each of the data runs, plotted as a function of focal pressure.

While the cavitation power generally agrees with the rate of temperature rise when an ensemble average of B is used, Fig. 4 shows that there is considerable variation when the proportionality constant for each individual measurement is plotted against the corresponding focal pressure. (The voltage gain of the power amplifier varied somewhat

from run-to-run, thus we observed small deviations in the focal pressure for repeated measurement using the same input voltage.) The proportionality relationship is particularly scattered at 3.5 and 2.5 MPa, and to a lesser degree at 3.3 MPa, where there appears to be a bifurcation in the value of *B*. Overall, *B* appears to decrease with increasing focal pressures.

Figure 5 shows the proportionality constant when the data is binned (±100 kPa) about the six pressures and the average fitting constant at the binned pressures is used to generate a fit of *B* with focal pressure. The fit corresponded to B = -90.5 x P_{foc} + 608 (R^2 = 0.5). The data are not strictly linear with pressure, so while it may not be valid to hold the proportionality relationship to such a fit, the trend is nonetheless present.

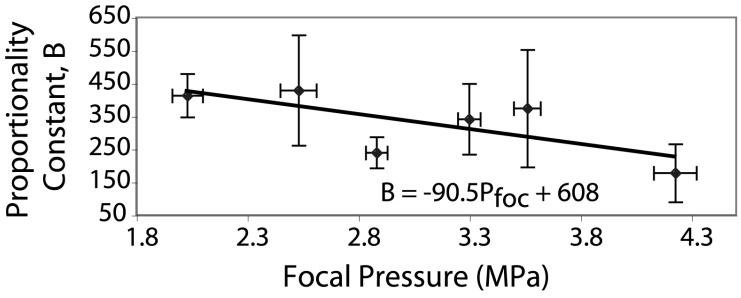

Figure 5: The mean cavitation power proportionality constant *B* as a function of pressure when the individual measurements are binned and averaged according to focal pressure (R^2 = 0.5). The vertical error bars represent the standard deviation of the proportionality constant at each focal pressure. The horizontal error bars represent the standard deviation of the focal pressure.

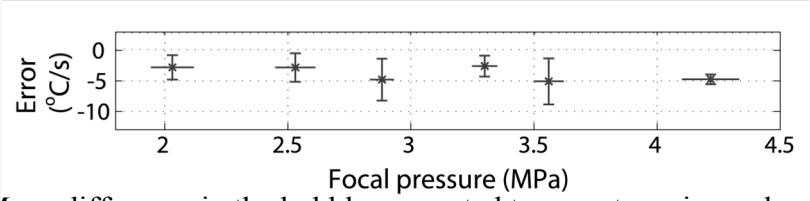

Figure 6: Mean difference in the bubble-generated temperature rise and cavitation power as a function of focal pressure.

The overall validity of B was evaluated by comparing the error in the difference of the fit, defined as

$$E(t) = \frac{\partial T_b}{\partial t} - B \cdot V_{rms}^2(t) \ . \tag{15}$$

The average error for a given measurement was given by $E_{avg} = \langle E(t) \rangle_t$, where t is the duration of the measurement and we employed the fitted value for B derived from Fig. 5. This was repeated for all 41 measurements and the results binned around the six focal pressures; results are shown in Fig. 6. The agreement is slightly better at the lower pressures and is generally within 5°C/s. The average difference between the rate of temperature rise and cavitation power was generally negative, indicating that the PCD-derived cavitation power consistently overestimated the temperature rise. Here, no attempt made to exclude or otherwise correct for artifacts associated with cavitation on the thermocouple tip.

DISCUSSION

The intent of this work was to evaluate whether a non-invasive measurement of broadband acoustic emissions can be used to monitor and assess accelerated heating from inertial cavitation during HIFU exposure. By employing idealized conditions, the number of independent parameters was reduced, leading to a better understanding of the underlying relationship between inertial cavitation emissions and heating from inertial cavitation. Since measurements were performed in homogeneous, non-perfused and well-characterized tissue phantoms, the amplitude of the fitting parameter B is not expected to describe all experimental scenarios, particularly not those encountered *in vivo*. Moreover, the pressure threshold for the onset of inertial cavitation was lower than in most tissue

types, allowing lower pressures to be employed and thus avoiding nonlinear effects on both the sound field and heating rates. At higher pressures, we expect a greater portion of the signal detected by the PCD will contain energy at the HIFU harmonic and super-harmonic frequencies, such that the underlying assumption that the conditioned PCD signal was dominated by energy from inertial cavitation would be violated. This scenario would require more a more sophisticated signal conditioning method, such as the comb filter approach, in order to isolate the energy from inertial cavitation [34]. While naturally-occurring *in vivo* pressure thresholds for inertial cavitation are significantly higher than those employed here, the inertial cavitation threshold for contrast agents used in thermal ablation studies, such as Optison™, are actually lower than the thresholds found in our media. Giesecke and Hynynen [11] detected inertial cavitation at ~0.4 MPa for the same 1.1 MHz frequency, compared to 1.4 MPa in the phantom employed here. Nevertheless, the results reported herein demonstrate that *the measurement of broadband cavitation noise provides a non-invasive, real-time, means for monitoring changes in heating rates from inertial cavitation.* This technique can be used to determine the onset of cavitation-enhanced heating and could have utility as a feedback parameter to control the HIFU treatment so that cavitation effects are either avoided or sustained. Moreover, it can be achieved using a clinical diagnostic imager configured to act as a spatially-resolved cavitation signal detector [34].

It is interesting to note that at the onset of sonication the cavitation power immediately displays elevated signal amplitudes, which is expected since the graphite in the phantom offers ample opportunity for prompt nucleation. After this the power gradually decreases, exhibiting elevated levels only when there is apparent cavitation on

the thermocouple. This decrease could be due to a number of factors. As the bubble field evolves, nuclei are "used up" [17], [35]-[37] and it can become increasingly difficult to sustain a set level of inertial cavitation without moving to a volume of previously unexposed phantom. Also, it is important to note that the equilibrium sizes of inertial cavitation bubbles are much smaller than resonance size [38]. As bubbles absorb gas due to rectified diffusion, their ability to grow unstably and collapse inertially is diminished due to the enhanced mass loading of the surrounding medium, resulting in a decrease in inertial cavitation activity over time. A third mitigating effect is ambient temperature. As the phantom heats up, the increase in vapor pressure inhibits inertial collapse [39], [40]. Indeed this imposes a fundamental limitation to the ability to sustain inertial bubble activity as the medium heats up. In hot mediums, the inertial cavitation field "shuts down" and is replaced by a scenario resembling boiling.

A detailed comparison of time-dependent heating rates and acoustically-measured cavitation powers reveal a number of deviations from the linear relationship suggested by Eq. (14), some of which may be artifactual. The noise power consistently overestimates the heating rate during the first 300 – 500 ms of the measurement, where $T_{amb} < T <$ 30°C. The thermocouple is displaced 0.5 mm from the axis of the HIFU beam and it is reasonable to assume that cavitation is most likely to occur initially along the beam axis. Given the finite thermal diffusivity of the phantom material, it not unrealistic to assume it will take time for the heat deposited by the very early stages of cavitation activity to reach the thermocouple. A 500 ms time delay corresponds to a thermal diffusion length of 0.28 mm, which is comparable to the distance from the axis to the thermocouple, particularly when the uncertainly in the precise location of initial bubble activity is

considered. This delay is an artifact consistent with the known measurement scheme and geometry.

In the measurements where cavitation nucleated on or near the thermocouple tip, the measured temperature rise during the cavitation burst was always higher than the corresponding cavitation power. We expect this is due to the fact that the thermocouple is a point-like sensor that is preferentially influenced by heat sources in its immediate vicinity, whereas the PCD senses pressure over a larger volume. The differences observed are to be expected and would not have occurred had we not inserted an invasive temperature sensor in the first place. A better approach would be to use a noninvasive sensing modality that allows estimates of average temperatures over specified volumes, such as MR thermometry.

Another measurement artifact we have yet to consider is viscous heating on the thermocouple tip, a prompt effect that will elevate the measured temperature by a fixed amount depending on the pressure amplitude. This supplemental heat acts as a bias that will impact the accuracy of the absolute temperature measurement but should not significantly affect the *rate* of temperature elevation for a short period (order of 100 ms) following the start of sonication. The additional heating could explain the initial overprediction of the heating rate, but is inconsistent with the subsequent observed underprediction. Realistically, the viscous heating artifact has generally resulted in temperature elevations on the order of a few degrees [29] at pressures below the cavitation threshold, so its overall impact relative to the rate of temperature rise is likely to be small. In addition, we attempted to minimize the effect by choosing a thermocouple with a diameter below the $\sqrt{\lambda}/5$ specification described by Hynynen and Edwards [41]

(where λ is the wavelength), orienting the thermocouple parallel to the HIFU acoustic axis, and positioning the thermocouple tip 0.5 mm away from the focus.

Finally, it is important to point out that the data presented in panel (b) of Figs. 2 and 3 *clearly demonstrate the ability of inertial cavitation to dramatically enhance heating in tissue-like material at relatively low HIFU focal pressures*. While there is no reason to believe that this effect cannot be duplicated in tissue, the paucity of cavitation nuclei in most tissues makes it difficult to initiate inertial cavitation at modest pressure amplitudes. Indeed, many treatment protocols mandate such high HIFU pressures (order 10 MPa) that other effects, such as nonlinear heating and boiling, tend to dominate. The *subtle* exploitation of cavitation-enhanced heating at low HIFU pressures necessitates the introduction of supplemental cavitation nuclei *in vivo*, or the use of large-amplitude, short-duration HIFU pulses to "pre-populate' the tissue with free bubble nuclei prior to exposure. These concepts are active areas of investigation [42]-[45].

SUMMARY AND CONCLUSIONS

The non-invasive acoustic measurement of cavitation power cannot account for all of the heating that occurs during HIFU sonication, especially if effects from conduction or perfusion, if present, are particularly strong. Nor can it predict the absolute temperature in the acoustic sensing region. However, cavitation power does appear to be proportional to the rate of temperature rise when the HIFU heating is accounted for and when nonlinear effects are small, as appears to be the case for the pressures employed in the agar-graphite phantoms. As such, the relationship between cavitation noise and supplemental heating from cavitation provides a basis for using intelligent cavitation

noise-sensing techniques as a noninvasive tool to monitor and assess enhanced heating from inertial cavitation generated during HIFU treatment.

ACKNOWLEDGEMENTS

The authors would like to thank Drs. Charles Thomas and Tianming Wu for helpful discussions, as well as financial support from The Gordon Center for Subsurface Sensing and Imaging Systems via NSF award number EEC-9986821 and the U.S. Army, Award Number DAMD17-02-2-0014 (The U.S. Army Medical Research Acquisition Activity, 820 Chandler Street, Fort Detrick, MD 21702-5014). The content of the information in this paper does not necessarily reflect the position or the policy of the Government.

APPENDIX A: Broadband signal analysis

The inertial cavitation measurement was based on the broadband PCD signal that was filtered below 5 MHz and was processed by a RMS signal converter. The measurement assumes that the signal above 5 MHz is composed chiefly of broadband inertial cavitation emissions and electronic noise, and that the nonlinear HIFU signal that was detected by the PCD was effectively removed by the highpass filter. This assumption was investigated by examining the spectral content of the PCD signal above 5 MHz. The PCD signal was amplified and conditioned with the 5 MHz high-pass filter (as described above and in Fig. 1) and digitized at 50 MSamples/s with a 14-bit digital oscilloscope (CompuScope 14100, Gage Corp., Lockport, IL). To isolate the spectrum of the broadband signal, a fast Fourier transform (FFT) was performed for each waveform. A digital comb filter was then applied to remove the energy at the HIFU harmonic and

super-harmonic frequencies (*nf, nf/2, ±nf/3*, where *f* is the fundamental frequency and *n* = *5, 6, ..., 12*). We employed a ±150 kHz band around each harmonic and a ±50 kHz band around each sub- and super-harmonic frequency. However, inertial cavitation noise was also present within these bands. To account for this, we assumed that since these bands are very narrow, the cavitation pressure is essentially constant across a given band. We therefore set the level of the spectrum in each of the filtered frequency bands equal to the level of unfiltered spectra just above a given filtered band. This technique is described in greater detail in Farny *et al.* [34].

After comb filtering, an inverse FFT was performed and the rms level of the isolated broadband component of the inertial cavitation signal was computed, along with the rms level of the unfiltered signal. The resulting bias error incurred by assuming that the unfiltered signal contained *only* broadband energy was given by:

$$\%error = \frac{V_{rms,unfil} - V_{rms,fil}}{V_{rms,unfil}}.$$

This bias error was determined for HIFU focal pressures ranging between 1.1 and 3.5 MPa; a total of 260 measurements were made in 4 phantoms. The error was found to be independent of pressure amplitude, possessed a mean value of about 3%, and minimum and maximum values of 2.1% and 5% respectively. This relatively low bias demonstrates that, at these HIFU pressures in agar-graphite phantoms, the sound power from the scattered HIFU signal above 5 MHz contributes minimally to the rms value of the detected PCD signal in the presence of cavitation.

REFERENCES

[1] S. A. Sapareto, and W. C. Dewey, "Thermal dose determination in cancer therapy," *Int J Radiat Oncol Biol Phys*, vol. 10, pp. 787-800, 1984.

[2] C. C. Church, "Thermal dose and the probability of adverse effects from HIFU," *Proc. 6th Int. Symp. Ther. Ultrasound*, edited by C. C. Coussios and G. ter Haar, Oxford, UK, American Institute of Physics, pp. 131-137, 2007.

[3] N. McDannold, K. Hynynen, D. Wolf, G. Wolf, and F. Jolesz, "MRI evaluation of thermal ablation of tumors with focused ultrasound," *J Magn Reson Im*, vol. 8, pp. 91-100, 1998.

[4] N. McDannold, C. M. Tempany, F. M. Fennessy, M. J. So, F. J. Rybicki, E. A. Stewart, F. A. Jolesz, and K. Hynynen, "Uterine leiomyomas: MR imaging-based thermometry and thermal dosimetry during focused ultrasound thermal ablation," *Radiology*, vol. 240, pp. 263-272, 2006.

[5] P. P. Lele, "Effects of ultrasound on 'solid' mammalian tissues and tumors in vivo," in *Ultrasound: Medical Applications, Bioeffects, and Hazard Potential*, edited by M. H. Repacholi, Plenum Press, NY, pp. 275-306, 1985.

[6] T. G. Leighton, *The Acoustic Bubble*, Academic Press, San Diego, CA, USA, 1997.

[7] K. Hynynen, "The threshold for thermally significant cavitation in dog's thigh muscle in vivo," *Ultrasound Med Biol*, vol. 17, pp. 157-69, 1991.

[8] R. G. Holt, and R. A. Roy, "Measurements of bubble-enhanced heating from focused, MHz-frequency ultrasound in a tissue-mimicking material," *Ultrasound Med Biol*, vol. 27, pp. 1399-1412, 2001.

[9] S. Hilgenfeldt, D. Lohse, and M. Zomack, "Sound scattering and localized heat deposition of pulse-driven microbubbles," *J. Acoust. Soc. Am*, vol. 107, pp. 3530-3539, 2000.

[10] D. Razansky, P. Einziger, and D. Adam, "Enhanced heat deposition using ultrasound contrast agent - modeling and experimental observations," *IEEE Trans. Ultrason. Ferroelectr. Freq. Control*, vol. 53, pp. 137-147, 2006.

[11] T. Giesecke, and K. Hynynen, "Ultrasound-mediated cavitation thresholds of liquid perfluorocarbon droplets in vitro," *Ultrasound Med Biol*, vol. 29, pp. 1359-1365, 2003.

[12] P. L. Edson, "The role of acoustic cavitation in enhanecd ultrasound-induced heating in a tissue-mimicking phantom," Ph.D. Dissertation, Boston University, 2001.

[13] R. G. Holt, and R. A. Roy, "Bubble dynamics in therapeutic ultrasound," in *Bubble and particle dynamics in acoustic fields: Modern trends and applications*, edited by A. A. Doinikov, Research Signpost, Kerala, India, pp. 183-229, 2005.

[14] X. M. Yang, R. A. Roy, and R. G. Holt, "Bubble dynamics and size distributions during focused ultrasound insonation," *J. Acoust. Soc. Am.*, vol. 116, pp. 3423-3431, 2004.

[15] E. C. Everbach, I. R. S. Makin, M. Azadniv, and R. S. Meltzer, "Correlation of ultrasound-induced hemolysis with cavitation detector output in vitro," *Ultrasound Med Biol*, vol. 23, pp. 619-624, 1997.

[16] W. Chen, A. Brayman, T. Matula, and L. Crum, "Inertial cavitation dose and hemolysis produced in vitro with or without Optison," *Ultrasound Med Biol*, vol. 29, pp. 725-37, 2003.

[17] W. S. Chen, A. A. Brayman, T. J. Matula, L. A. Crum, and M. W. Miller, "The pulse length-dependence of inertial cavitation dose and hemolysis," *Ultrasound Med Biol*, vol. 29, pp. 739-48, 2003.

[18] J. Seo, B. C. Tran, T. L. Hall, J. B. Fowlkes, G. D. Abrams, M. O'Donnell, and C. A. Cain, "Evaluation of ultrasound tissue damage based on changes in image echogenicity in canine kidney," *IEEE Trans Ultrason Ferroelectr Freq Control*, vol. 52, pp. 1111-20, 2005.

[19] V. A. Khokhlova, M. R. Bailey, J. W. Reed, B. W. Cunitz, P. J. Kaczkowski, and L. A. Crum, "Effects of nonlinear propagation, cavitation, and boiling in lesion formation by high intensity focused ultrasound in a gel phantom," *J Acoust Soc Am*, vol. 119, pp. 1834-48, 2006.

[20] I. M. Hallaj, and R. O. Cleveland, "FDTD simulation of finite-amplitude pressure and temperature fields for biomedical ultrasound," *J. Acoust. Soc. Am.*, vol. 105, pp. l7-l12, 1999.

[21] P. J. Westervelt, "Parametric Acoustic Array," *J. Acoust. Soc. Am.*, vol. 35, pp. 535-537, 1963.

[22] M. F. Hamilton, and D. T. Blackstock, *Nonlinear Acoustics*, Academic Press, San Diego, CA, USA, 1998.

[23] H. H. Pennes, "Analysis of tissue and arterial blood temperatures in the resting human forearm," *J Appl Physiol*, vol. 1, pp. 93-122, 1948.

[24] A. Pierce, "Acoustics: An introduction to its physical principles and applications," pp. 515-519, 1994.

[25] J. Devin, "Survey of Thermal, Radiation, and Viscous Damping of Pulsating Air Bubbles in Water," *J. Acoust. Soc. Am.*, vol. 31, pp. 1654-1667, 1959.

[26] A. Prosperetti, "Thermal effects and damping mechanisms in the forced radial oscillations of gas bubbles in liquids," *J. Acoust. Soc. Am.*, vol. 61, pp. 17-27, 1977.

[27] V. Kamath, H. N. Oguz, and A. Prosperetti, "Bubble oscillations in the nearly adiabatic limit," *J. Acoust. Soc. Am.*, vol. 92, pp. 2016-2023, 1992.

[28] L. Kondić, J. I. Gersten, and C. Yuan, "Theoretical studies of sonoluminescence radiation: Radiative transfer and parametric dependence," *Phys. Rev. E*, vol. 52, pp. 4976, 1995.

[29] J. Huang, R. G. Holt, R. O. Cleveland, and R. A. Roy, "Experimental validation of a tractable numerical model for focused ultrasound heating in flow-through tissue phantoms," *J. Acoust. Soc. Am.*, vol. 116, pp. 2451-2458, 2004.

[30] J. Huang, "Heating in vascular and flow-through tissue phantoms induced by focused ultrasound," Ph.D. Dissertation, Boston University, 2002.

[31] X. Gong, Z. Zhu, T. Shi, and J. Huang, "Determination of the acoustic nonlinearity parameter in biological media using FAIS and ITD methods," *J. Acoust. Soc. Am.*, vol. 86, pp. 1-5, 1989.

[32] C. H. Farny, "Identifying and monitoring the roles of cavitation in heating from high-intensity focused ultrasound," Ph.D. Dissertation, Boston University, 2007.

[33] B. A. Rabkin, V. Zderic, and S. Vaezy, "Hyperecho in ultrasound images of HIFU therapy: involvement of cavitation," *Ultrasound Med Biol*, vol. 31, pp. 947-56, 2005.

[34] C. H. Farny, R. G. Holt, and R. A. Roy, "Temporal and spatial detection of HIFU-induced inertial and hot-vapor cavitation with a diagnostic ultrasound system," *Ultrasound Med Biol*, vol. 35, pp. 603-615, 2009.

[35] T. G. Leighton, M. J. W. Pickworth, A. J. Walton, and P. P. Dendy, "Studies of the cavitational effects of clinical ultrasound by sonoluminescence: 1. Correlation of sonoluminescence with the standing wave pattern in an acoustic field produced by a therapeutic unit," *Phys Med Biol*, vol. 33, pp. 1239-1248, 1988.

[36] M. J. W. Pickworth, P. P. Dendy, T. G. Leighton, and A. J. Walton, "Studies of the cavitational effects of clinical ultrasound by sonoluminescence: 2. Thresholds for sonoluminescence from a therapeutic ultrasound beam and the effect of temperature and duty cycle," *Phys Med Biol*, vol. 33, pp. 1249-1260, 1988.

[37] T. G. Leighton, "Bubble population phenomena in acoustic cavitation," *Ultrason Sonochem*, vol. 2, pp. s123-136, 1995.

[38] C. C. Coussios, and R. A. Roy, "Applications of acoustics and cavitation to noninvasive therapy and drug delivery," *Annu Rev Fluid Mech*, vol. 40, pp. 395-420, 2008.

[39] Y. Hao, and A. Prosperetti, "The dynamics of vapor bubbles in acoustic pressure fields," *Phys Fluid*, vol. 11, pp. 2008-2019, 1999.

[40] C. H. Farny, R. G. Holt, and R. A. Roy, "Monitoring the development of HIFU-induced cavitation activity," *Proc. 5th Int. Symp. Ther. Ultrasound*, edited by G. T. Clement, N. McDannold, and K. Hynynen, Boston, MA, American Institute of Physics, pp. 348-352, 2006.

[41] K. Hynynen, and D. K. Edwards, "Temperature measurements during ultrasound hyperthermia," *Med Phys*, vol. 16, pp. 618-26, 1989.

[42] S. D. Sokka, R. King, and K. Hynynen, "MRI-guided gas bubble enhanced ultrasound heating in in vivo rabbit thigh," *Phys Med Biol*, vol. 48, pp. 223-41, 2003.

[43] C. H. Farny, T. M. Wu, R. G. Holt, T. W. Murray, and R. A. Roy, "Nucleating cavitation from laser-illuminated nano-particles," *Acoust. Res. Lett. Onl.*, vol. 6, pp. 138-143, 2005.

[44] T. Wu, "Bubble mediated focused ultrasound: Nucleation, cavitation dynamics and lesion prediction," Ph.D. Dissertation, Boston University, 2006.

[45] B. Krasovitski, H. Kislev, and E. Kimmel, "Modeling photothermal and acoustical induced microbubble generation and growth," *Ultrasonics*, vol. 47, pp. 90-101, 2007.